Gap junction assembly: roles for the formation plaque and regulation by the C-terminus of connexin43

Ross G. Johnson[a], James K. Reynhout[b], Erica M. TenBroek[a,*], Bradley J. Quade[a,†], Thomas Yasumura[c], Kimberly G. V. Davidson[c], Judson D. Sheridan[a], and John E. Rash[c]
[a]Department of Genetics, Cell Biology and Development, University of Minnesota, Minneapolis, MN 55455; [b]Department of Biology, Bethel University, St. Paul, MN 55112; [c]Department of Biomedical Sciences, Colorado State University, Fort Collins, CO 80523

ABSTRACT **Using an established gap junction (GJ) assembly system with experimentally re-aggregated cells, we analyzed "formation plaques" (FPs), apparent sites of GJ assembly. Employing freeze-fracture electron microscopy methods combined with filipin labeling of sterols and immunolabeling for connexin43 (Cx43), we demonstrated that FPs constitute distinct membrane "domains" and that their characteristic 10-nm particles contain connexin43, thus representing precursors (i.e., GJ hemichannels) engaged in assembly. Analysis of FPs in new systems—HeLa and N2A cells—resolved questions surrounding several key but poorly understood steps in assembly, including matching of FP membranes in apposed cells, reduction in the separation between FP membranes during assembly, and the process of particle aggregation. Findings also indicated that "docking" of GJ hemichannels occurs within FP domains and contributes to reduction of intermembrane separation between FPs. Other experiments demonstrated that FPs develop following a major C-terminal truncation of Cx43 (M257), although assembly was delayed. Particle aggregation also occurred at lower densities, and densities of particles within developing GJ aggregates failed to achieve full-length levels. With regard to regulation, inhibition of assembly following protein kinase C activation failed to occur in the M257 truncation mutants, as measured by intercellular dye transfer. However, several C-terminal serine mutations failed to disrupt inhibition.**

Monitoring Editor
Alpha Yap
University of Queensland

Received: Feb 17, 2011
Revised: Oct 18, 2011
Accepted: Oct 25, 2011

INTRODUCTION

Connexins, which form cell-to-cell channels found in vertebrate gap junctions (GJs), are required for the normal function of virtually all types of cells, tissues, and organs (Locke and Harris, 2009). Fundamental insights have come from studying connexin deletions in mice, as well as connexin mutations that are linked to a number of human diseases (Dobrowolski and Willecke, 2009). This compelling evidence emphasizes how various connexins play different roles. This is partially explained by the fact that channels formed by different connexins or connexin combinations display qualitatively different permeability properties and are regulated differently (Beyer *et al.*, 2001; Burt and Steele, 2003; Weber *et al.*, 2004). Thus connexin diversity provides for important qualitative variations in cell-to-cell communication.

Similarly, quantitative variations in GJ communication also play critical roles, for example, in development (Wei *et al.*, 2004), cell growth (Cronier *et al.*, 2009), and a range of cellular responses (Paemeleire *et al.*, 2000). Some of these variations likely arise from modifications in GJ assembly, a premise that is consistent with the exceptionally short half-lives of connexins (often just several hours) in different cell systems (Fallon and Goodenough, 1981; Beardslee *et al.*, 1998) and the rapid remodeling and reassembly of GJs seen in steady-state cultures (Simek *et al.*, 2009). Accordingly, the regulation of GJ assembly is likely to be an important way for cells to control GJ structure and function.

This article was published online ahead of print in MBoC in Press (http://www.molbiolcell.org/cgi/doi/10.1091/mbc.E11-02-0141) on November 2, 2011.

Present addresses: *Therapy, Research and Development, Medtronic, Fridley, MN 55432; †Brigham and Women's Hospital, Boston, MA 02115.

Address correspondence to: Ross G. Johnson (gaplab@umn.edu).

Abbreviations used: Cx43, connexin43; EM, electron microscopy; FF, freeze-fracture; FP, formation plaque; FRIL, freeze-fracture replica immunolabeling; GJ, gap junction; PKC, protein kinase C; TPA, 12-*O*-tetradecanylphorbol-13-acetate.

A long-term goal of our research has been to elucidate the process, mechanisms, and regulation of GJ assembly (Meyer *et al.*, 1992; Lampe, 1994; Paulson *et al.*, 2000; TenBroek *et al.*, 2001; Johnson *et al.*, 2002). Our approach has been to use structural (freeze-fracture [FF] and electron microscopy [EM]) and physiological (electrical coupling and dye transfer) methods to study GJ assembly among dissociated, recovered, and reaggregated cells (Johnson *et al.*, 1974; Preus *et al.*, 1981b). Although the model is generally supported by our earlier studies (Johnson *et al.*, 1974; Preus *et al.*, 1981b) and by others (Decker and Friend, 1974; Risinger and Larsen, 1983; Fujimoto *et al.*, 1997), certain key features remained unclear, and these are emphasized in the first part of the present study. Moreover, we confirmed that the model, based heavily on earlier studies of Novikoff hepatoma cells, is also useful in describing assembly in two new systems—transfected HeLa and N2A cells—and is thus more likely to reflect the essential steps in de novo GJ assembly elsewhere.

In our model, we proposed that formation plaques (FPs) are distinct membrane domains, but this contention was based on subjective rather than molecular evidence. To obtain objective molecular information about FPs, we used two different approaches in the present study. First, we used filipin labeling (Elias *et al.*, 1979) to evaluate hydroxysterol levels (i.e., largely cholesterol) within the membranes of reaggregated Novikoff hepatoma cells, reasoning that changes in membrane lipids in FPs might facilitate or regulate assembly (Malewicz *et al.*, 1990; Meyer *et al.*, 1991). FPs were notably deficient in filipin labeling, suggesting either a deficiency of cholesterol or inaccessibility of the sterol for filipin binding. Second, we used powerful freeze-fracture replica immunolabeling (FRIL) methods (Li *et al.*, 2008) to localize connexin43 (Cx43) proteins within developing FPs, taking advantage of large FPs found in Cx43-transfected N2A cells. Together these analyses demonstrate both the specialized nature of FP membranes and the role of FPs as the sites of accumulation of GJ precursors (namely, connexons or GJ hemichannels) during GJ assembly.

The larger and/or more distinctive FPs also allowed us to obtain more definitive support for several other key aspects of our assembly model, including the matching of FPs in apposed cells, the enrichment of 10-nm particles, the depletion of smaller particles in FPs, the steps in the aggregation of 10-nm particles ultimately into GJs, and the progressive reduction of the distance between FP membranes. Moreover, quantitative FF analysis of other FP parameters, such as FP area and the number, degree of aggregation, and density of 10-nm particles, provided more, sometimes unexpected, information on the processes of initiation, maturation, and growth of FPs.

In the next part of our study, we turned our attention to the role of the cytoplasmic, C-terminal tail (CT tail) of Cx43, first in basal and then in negatively regulated assembly. Previous studies showed that cells without the CT tail could still form GJs and develop dye permeability but at an apparently slower rate (TenBroek *et al.*, 2001; Maass *et al.*, 2004, 2007; Simek *et al.*, 2009). However, none of these earlier studies used FF to study the development of FPs in the absence of the CT tail. Using N2A and HeLa cells expressing a truncated version of Cx43 (M257), we compared FP development with that in the full-length Cx43 transfectants during basal GJ assembly. We found only very limited FP development in the N2A-M257 cells but detected most assembly steps in the HeLa-M257 cells. However, a more detailed quantitative comparison of the HeLa-M257 and HeLa-Cx43 cells showed more complex results and revealed important new features of FP development. Although the M257 cells had an apparent delay in the overall development of FPs, the aggregation of particles appeared to occur at a lower density of unaggregated particles than in the HeLa-Cx43 cells, implying a higher efficiency of aggregation in the M257. Yet the resulting aggregates were less tightly packed (i.e., lower particle density within the aggregates) than in the HeLa-Cx43 cells and did not show a gradual increase in density with assembly time, in contrast to that seen in the HeLa-Cx43 cells.

The quantitative differences in assembly by the Cx43 and M257 cells suggest that FP development and GJ maturation may require interactions of the CT tail of Cx43 with other connexin moieties or other protein(s) (Laird, 2010). Interactions with other proteins have been postulated to affect many features of Cx43 function, including GJ assembly (Hunter *et al.*, 2005) and may be the focus of regulation, occurring, for example, through phosphorylation of various sites on the CT tail (Solan and Lampe, 2009). Earlier work demonstrated that the CT tail is required for the positive regulation of GJ assembly—the "enhanced assembly" that is mediated by cAMP (Paulson *et al.*, 2000; TenBroek *et al.*, 2001). In addition, phosphorylation of Cx43 by casein kinases at sites within the CT tail has been shown to influence GJ assembly (Cooper and Lampe, 2002). However, it was not known whether the negative regulation of GJ assembly by means of protein kinase C (PKC) activation via the phorbol ester 12-*O*-tetradecanylphorbol-13-acetate (TPA; Lampe, 1994) requires full-length Cx43. Our dye injection studies here of assembly by the M257 truncation mutants demonstrate that the CT tail is required for the TPA effect. Moreover, our detailed analysis of various phosphorylation-site mutants raises the interesting possibility that the PKC effect on GJ assembly does not require phosphorylation of Cx43 at a specific site(s) on the CT tail but rather an interaction between the CT tail and another protein affected by PKC, for example, one involved in membrane trafficking.

RESULTS

Molecular evidence that formation plaques are distinct plasma membrane domains

Probing FP membrane cholesterol: filipin labeling. The relatively flat, apparently rigid topology of FPs suggests that the composition or structure of membrane lipids may be altered and somehow contribute to early steps in FP assembly (Johnson *et al.*, 1974). Prompted by early findings of significant cholesterol levels in isolated GJ fractions (Henderson *et al.*, 1979) and evidence that cholesterol can affect membrane fluidity (Malewicz *et al.*, 1990), we sought to determine whether FPs have different levels of membrane cholesterol than the surrounding, nonjunctional plasma membrane. We applied a convenient FF-EM method for mapping the distribution of cholesterol in membranes, using the polyene antibiotic filipin, which is known to bind specifically to β-hydroxysterols and to be useful in probing membrane domains (Elias *et al.*, 1979).

In FF replicas of reaggregated Novikoff hepatoma cells (Johnson *et al.*, 1974), filipin-induced P-face protrusions were distributed widely throughout the plasma membrane (Figure 1 and Table 1). However, unexpectedly, filipin-based protrusions were totally missing from FP membranes, whether or not they contained aggregated particles, that is, small, immature GJs (Figure 1, A and B). In this regard, they behaved similarly to mature GJs, which also excluded filipin (Figure 1C), as reported earlier (Elias *et al.*, 1979; Risinger and Larsen, 1983). However, recent studies revealed filipin labeling of a subset of GJs in the lens (Biswas and Lo, 2007), reinforcing the concept that filipin can be used to probe GJs and FPs for cholesterol. Of importance, filipin treatment in the present study did not appear to alter the proportion of FPs containing particle aggregates, the mean number of aggregated particles per FP or the mean area of FPs (Table 1). This makes it unlikely that filipin treatment obscured or altered the nature of FPs, causing a certain class of FPs to be overlooked during

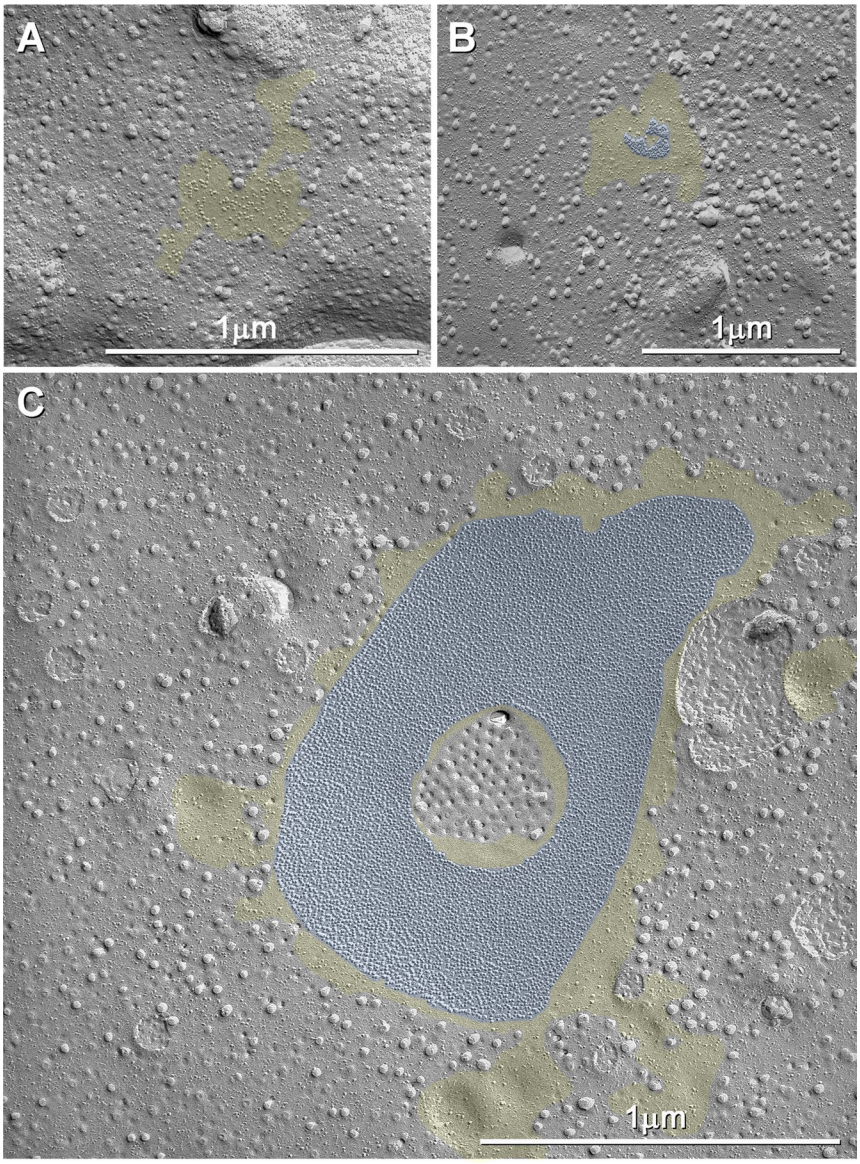

FIGURE 1: Filipin labeling of experimentally reaggregated Novikoff hepatoma cells. All images from transmission electron microscope (TEM) analysis of FF replicas. Note the protrusions from the membrane created by the filipin binding to β-hydroxysterols, largely in the form of cholesterol, and predominantly at the cytoplasmic surface of the plasma membrane. (A) In an FP(−) with only unaggregated particles, filipin label is observed surrounding the FP (yellow overlay) but not within it. (B) Filipin labeling also fails to extend into this FP (yellow overlay), which contains a small GJ aggregate (blue overlay). (C) A large GJ in a filipin-labeled cell (blue overlay), with no filipin labeling of the particle aggregate, consistent with a previous report (Elias *et al.*, 1979) but with filipin binding in a particle-free zone within the GJ. Of interest, the polarity/direction of membrane curvature of filipin labeling at this site (numerous depressions on the P-face) was opposite that found typically in the nonjunctional plasma membrane, which surrounds the GJ (largely protrusions on the P-face). Note the paucity of 10-nm particles in the area surrounding this mature GJ (yellow overlay). Calibration bars, 1.0 μm.

microscopic examination. Thus the lack of filipin binding appears to be a consistent and significant property of FP membranes, providing evidence that the FP is a specialized membrane domain in which cholesterol is either deficient or inaccessible for filipin binding.

Probing FP connexins: immunolabeling of freeze-fracture replicas. Another distinguishing characteristic of FP membranes is the accumulation of uniform, 10-nm intramembranous particles. If, as we propose, these particles are GJ precursors, they should be composed of connexins. To test this idea, we next used FRIL methods (Fujimoto, 1995; Rash and Yasumura, 1999) and transmission EM to study reaggregated HeLa and N2A cells transfected with Cx43 to determine whether Cx43 is enriched in the FPs and associated with the 10-nm particles. With the use of antibodies specific for the C-terminal tail of Cx43, which resides on the cytoplasmic side of the membrane, along with secondary gold-labeled antibodies, Cx43-containing GJs can be labeled on the surface that underlies the P-fracture face (Rash *et al.*, 2005). Our results with this approach are illustrated in Figure 2A**,** which shows several small GJs and FPs immunolabeled with 20-nm gold beads. One FP (Figure 2B, yellow overlay) clearly shows labeling associated with a group of unaggregated particles, most of which measured ~10 nm in diameter, as well as labeling of a nearby GJ. Other examples are shown in Figure 2, C–E. Thus the Cx43 labeling was associated with both the dispersed and aggregated 10-nm particles within the FPs (also see *Discussion*).

The specificity of the immunogold labeling was illustrated in several ways. First, the background labeling was exceptionally low (Figure 2, A–E). Second, all of the labeling of the protoplasmic fracture face (P-face) was, in fact, always on the tissue side of the replica, that is, the former cytoplasmic side of the membrane (as predicted based on the location of the epitope, and as confirmed using specimen tilt in the EM along with stereoscopic viewing) and never on the opposite, Lexan-coated surface of the replica. Third, using a primary monoclonal antibody for Cx43, it was possible to use two different secondary antibodies tagged with different sizes of gold to probe the distribution of Cx43. A large FP with multiple particle aggregates was labeled with two sizes of gold beads that localize Cx43 in Figure 2E (blue overlay); note the overlap of the two gold signals. It should also be emphasized that no other membrane specializations bound the antibodies for Cx43. We conclude that the labeling of the FPs was highly specific.

Consistent with the specificity, the extraplasmic fracture faces (E-faces) of junctional membranes were also labeled, including pits derived from small aggregates (Figure 2D), as well as multiple sites within larger FPs. Thus our interpretation is that the unaggregated 10-nm particles found in FPs contain Cx43 and therefore are GJ precursors (connexons or hemichannels).

Phases in the development of formation plaques

Our model for GJ assembly (see *Introduction*), which emphasizes the role of FPs, was derived almost exclusively from studies of reaggregated Novikoff hepatoma cells (Johnson *et al.*, 1974; Preus *et al.*, 1981b). These early studies provided significant support for certain features of FP development proposed in the model, such as the early appearance of FPs, the increase in numbers of 10-nm particles and particle aggregates with assembly time, and the

	Control	Filipin-treated samples	*t* test
Plaques examined (n values)	25 (100%)	51 (100%)	NA
FP(–)s	19 (76%)	35 (68%)	NA
FP(+)s	6 (24%)	16 (31%)	
Area of FP(–)s (geometric mean in μm^2, ± SEM)	0.087 0.078–0.098	0.073 0.065–0.081	0.33 Not significant
Area of FP(+)s (geometric mean in μm^2, ± SEM)	0.133 0.102–0.170	0.123 0.100–0.151	0.84 Not significant
Mean area of all FPs (geometric mean in μm^2, ± SEM)	0.096 0.085–0.107	0.086 0.076–0.096	0.51 Not significant
Number of aggregated particles/FP(+) (geometric mean)	25 14–44	27 21–33	0.90 Not significant
Filipin profiles per μm^2 of plasma membrane in nonplaque areas	NA	155 ± 9 (n = 6)	

The percentages of FP(−)s are similar in the two samples. In addition, the mean number of aggregated particles and the mean areas of plaques (expressed as geometric means; see *Materials and Methods*) are not significantly different following filipin treatment; values for Student's *t* test are shown in the final column. The quantitative data argue against this, as FP areas on average would then vary with filipin treatment, and they do not. Thus the FPs observed in the filipin-treated samples display features similar to those in the control sample. This indicates that it is unlikely the filipin treatment altered the appearance of FPs, contributing to a biased sample. One could also envision a variation in binding such that early FPs retained the filipin labeling (like nonjunctional membranes) and only more mature, larger FPs would be devoid of filipin. However, no support was found for this idea. Filipin profiles per μm^2 are expressed as the arithmetic mean ± SEM.

TABLE 1: Quantitative analysis of formation plaques in filipin-treated samples.

progressive decrease in the proportion of unaggregated particles. However, several key features were less well supported, including 1) the matching of FP membranes in apposed cells, 2) the enrichment of 10-nm particles and depletion of smaller particles in FPs, 3) the process of particle aggregation, including the fate of small aggregates, and 4) a reduction in the separation between FP membranes during assembly. Moreover, the applicability of the model to GJ assembly in other cell systems has been uncertain. In the present study, using transfected HeLa and N2A cells, we obtained evidence for important but poorly supported parts of the model while confirming the generality of the model in two additional cell systems.

Matching of FPs. The question of whether an FP membrane in one cell is matched with a similar structure in an apposed cell has been difficult to resolve with confidence. This is because the answer requires a view of both membranes, and with small and infrequent FPs the chance that the fracture plane will skip from one membrane to another in the middle of the FP is exceedingly limited. Thus replicas of N2A and HeLa cells had the potential of providing major insights into the question of whether FPs develop in a coordinated manner between two apposed membranes, an important feature of the FP model. In fact, we found more than 100 examples in which fractures skipped between membranes, often multiple times within an FP (e.g., Figure 3). In these cases, the specializations in one FP membrane were consistently found to be similar to those in the apposed membrane, with regions of clustered E-face pits adjacent to regions of clustered P-face particles or aggregated E-face pits continuous with aggregated P-face particles. All of these observations support the idea of matched FP membranes, although the basis for this cooperative interaction between membranes in early FPs remains unclear.

Enrichment of large and depletion of small FP particles. Two fundamental features of the assembly model are the accumulation in FPs of 10-nm particles, which, according to our FRIL studies (discussed earlier) contain Cx43, and the depletion of smaller particles. Figure 3 shows several large FPs with different densities of uniformly sized 10-nm particles, both unaggregated and aggregated, and variable loss of smaller particles. The images are consistent with differing stages in 10-nm particle enrichment (cf. Figure 3, A and B) and small-particle depletion (Johnson *et al.*, 1974). However, to add new quantitative support for these subjective interpretations, the numbers of both 10-nm particles and smaller particles were determined in a series of plaques at different stages in development, as well as in nonjunctional membranes. The results from one method are illustrated in Supplemental Figure S1. Similar results were obtained with a second method, which evaluated entire FP membranes. Whereas 10-nm particles were found to comprise from 6 to 27% of the particles in nonjunctional membranes, they represented 76–94% of the particles in FP membranes, both per unit area, an "enrichment" of up to ~12-fold in FPs of higher density. There was also a "depletion" of smaller particles, down to as few as 6% of the FP particles. Both features underscore the fact that FP membranes represent specialized domains.

Aggregation of 10-nm particles. Another important feature of the assembly model is the aggregation of 10-nm particles in FPs, as illustrated in Figure 3. Aggregates took a variety of shapes, often elongated (Figure 3, A and B), and sometimes lacy (Figure 3C), which may represent an early stage of particle aggregation. E-Face fractures of other lacy aggregates (Figure 3D) provide insight into the topography of the developing FPs. In other FPs (Figure 3E), large numbers of aggregates were observed, implying many different nucleation sites for aggregation. In some cases, particle-free areas were found within the larger networks of aggregated particles (e.g., Figure 3, B and C), consistent with the idea that unaggregated 10-nm particles have been incorporated into the aggregates. Of interest, membrane invaginations have been detected within particle aggregate regions (Figure 3E, inset), representing membrane vesicles either fusing with the FP membrane or pinching off, as in exocytosis and endocytosis, respectively. This constitutes the FP version of membrane trafficking, described previously for GJ membranes (Gaietta *et al.*, 2002; Shaw *et al.*, 2007).

In addition, earlier reports provided evidence for the lateral fusion of small-particle aggregates, thereby reducing their number and increasing the number and size of larger aggregates and creating more mature GJs (Preus *et al.*, 1981b). Our analysis of the much larger FPs in the N2A system provided a second important line of support for the fusion hypothesis. In a number of cases, developing FPs each displayed several dozen particle aggregates

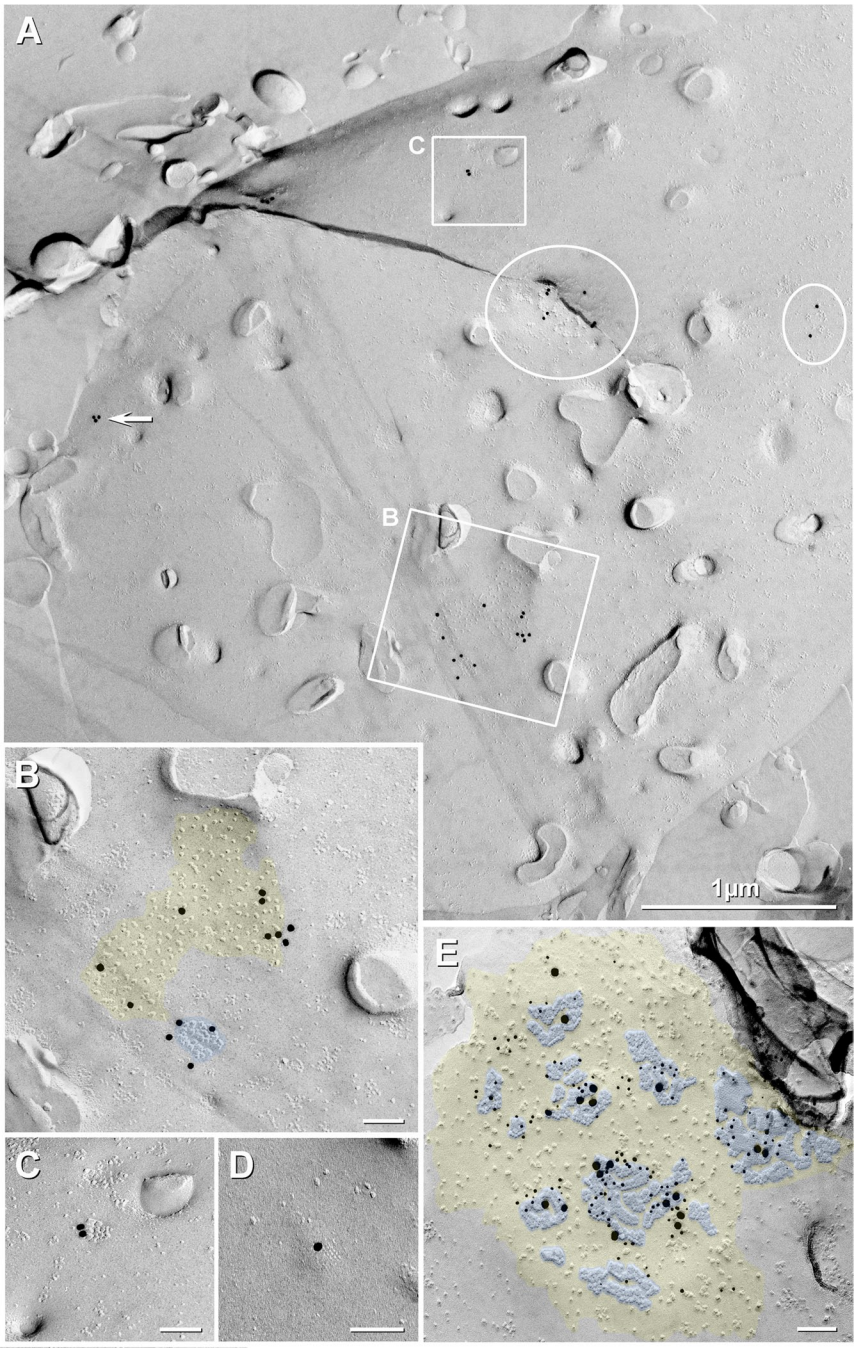

FIGURE 2: FRIL images of HeLa cells (clone Cx43-K) (A–D) and N2A cells (E) stably transfected with Cx43, and reaggregated to enhance FP development. All images are from TEM analysis of the immunolabeled replicas; see *Materials and Methods* for FRIL details. Cx43 was detected with a monoclonal antibody and 20-nm, gold-labeled secondary antibodies (A–D) or 10- and 20-nm gold labels (E). (A) Low-magnification view of a labeled HeLa cell plasma membrane, illustrating low background labeling. Boxes show specific labeling of GJs and an FP, enlarged as B and C. Ovals in A designate additional FPs. Arrow, nonspecific labeling as revealed by stereoscopic viewing (not shown) to be on the Lexan-coated side of the replica. (B) Labeled GJ that is relatively small (blue overlay), adjacent to a modest FP (yellow overlay). Note that most of the unaggregated particles in the FP are of a relatively large and uniform size (~10 nm). (C) Labeling of a very small GJ with two gold particles illustrates the sensitivity of the methods. (D) A small GJ is labeled on the E-face with a single gold particle. (E) Labeling with Cx43 antibody, detected by two sizes of gold-tagged secondary antibodies (10- and 20-nm gold). Note the overlap of the two sizes of gold within the large FP (yellow overlay), involving label on both unaggregated particles and aggregates (blue overlay). The aggregates contain higher particle densities and correspondingly higher labeling densities. Note that with the two antibody steps used here (primary and secondary antibodies), gold particles were found within 28 nm (most within 15 nm) of the labeled antigenic sites (Fujimoto, 1995; Fujimoto *et al.*, 1997; Kamasawa *et al.*, 2006). Small calibration bars, 0.1 μm.

(e.g., Figure 3E). It seems highly unlikely that each of these aggregates would develop into an individual GJ, because we never observed more than a few large, mature GJs in a single N2A cell expressing Cx43. These findings complement fluorescence studies on the lateral mobility of connexins within the plasma membrane (Simek *et al.*, 2009). Aggregate fusion is consistent with a biophysical model for GJ structure, which emphasizes the minimization of the repulsive forces between apposed membranes through the side-by-side aggregation of docked channels (Braun *et al.*, 1984).

Reduction of intermembrane space between FPs. FF analysis also validated another key feature of the assembly model—a progressive reduction in the distance between matched FP membranes. These separations appeared to fall into three classes. Early FPs (defined by smaller areas and lower particle densities) exhibited a rather broad separation, with an intermembrane distance interpreted as 10–20 nm and approaching that of apposed, nonjunctional membranes; we found 33 examples of this class. The aggregates of particles in FPs displayed a second class. Whenever the fracture planes skipped between these membranes (63 examples), the separations were much reduced, as in a mature GJ where the distance measures ~2 nm (Figure 3, E and F). Finally, images were also obtained of a third type of separation (Figure 3C), involving a reduced extracellular space (comparable to a mature GJ), but in FP areas containing unaggregated particles, with no evidence of aggregates (18 examples). We believe that these less frequent images represent an intermediate in the process by which the intermembrane space is reduced. In no instance did we observe an aggregate with a broad membrane separation. Thus our interpretation is that FP development clearly includes a process that reduces the intermembrane distance found in early FPs.

Hemichannel docking would provide a logical mechanism for converting the broad class of membrane separations to the narrow class associated with particle aggregates and GJs. Strong support for this idea comes from E-face views of lacy particle aggregates (Figure 3D and Supplemental Figure S2), which reveal grooves or valleys, indicating that the intermembrane separation is sharply reduced and precisely at the site of particle aggregation. In addition, small numbers of hexagonally arrayed pits (reflecting small aggregates) were found in depressed sites on E-faces,

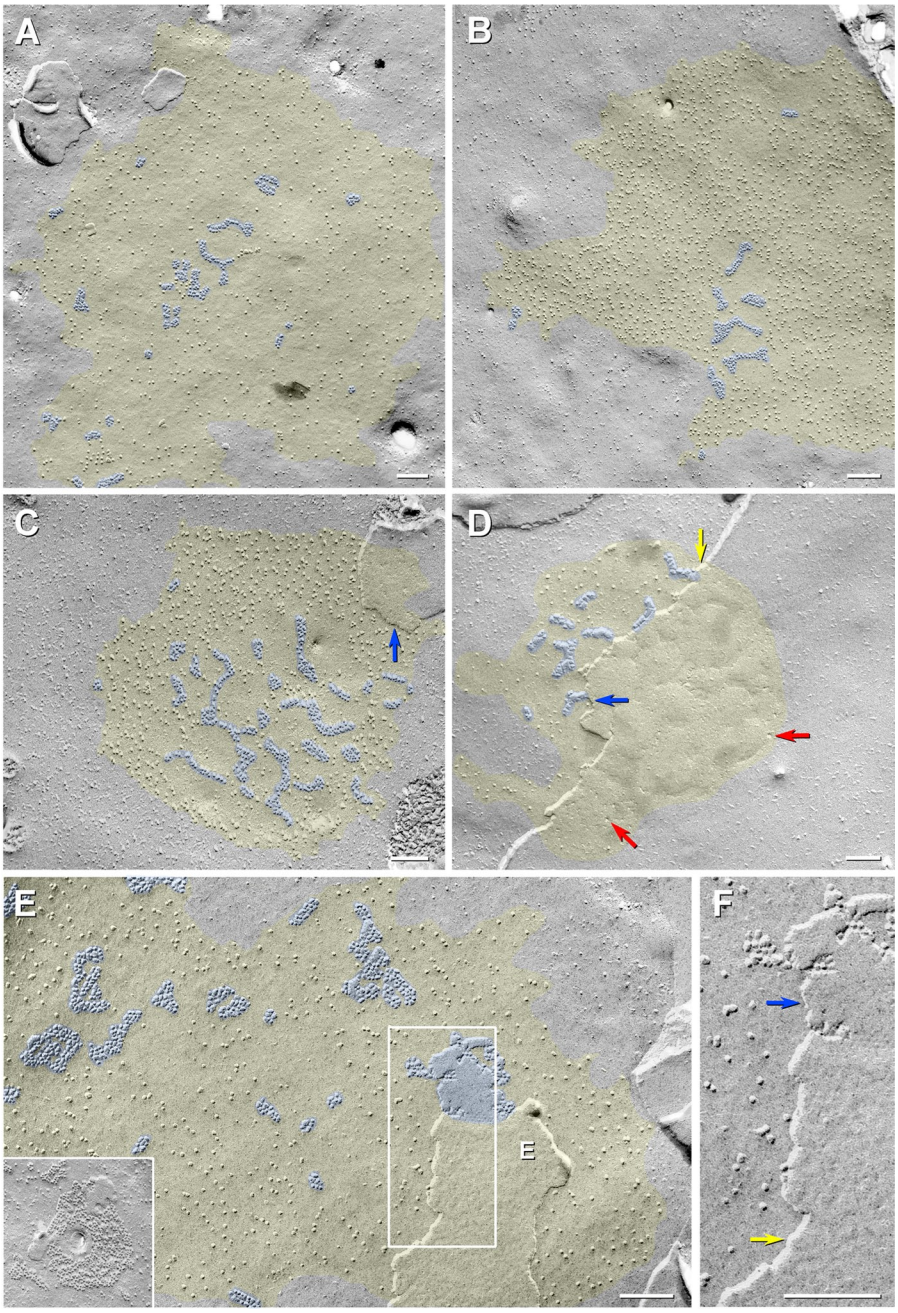

FIGURE 3: Images from FF replicas of N2A cells, expressing full-length Cx43, and reaggregated for 3 h. (A) Large FP with a modest number of unaggregated particles (yellow overlay) and several particle aggregates (small GJs, blue overlays). (B) FP illustrating a dramatic number of unaggregated particles (yellow overlay) and a few particle aggregates (blue overlay). (C) Lacy particle aggregates (blue overlay) are found within this FP (yellow overlay). Note the relatively "clear" areas surrounding some of the particle aggregates and the fragment of E-face in the upper right, which provides an indication of the separation between apposed membranes (arrow). (D) A lacy aggregate, as in C, but in this case both P- and E-faces are involved, providing a clear example of matched membrane specializations within the FP and insight into membrane topography. A blue arrow identifies a narrow membrane separation, the yellow arrow a broader separation. Red arrows also point to two especially large pits on the E-face, one near the end of a clear groove or valley and the other in a region with multiple smaller pits. (E) Part of an unusually large FP (yellow overlay) with many (total, >50, not all shown) particle aggregates (blue overlay) and a fragment of the apposed membrane that illustrates membrane separation (labeled E). The inset shows part of a large FP with a sizeable aggregate (blue overlay), in the center of which is seen a membrane vesicle fusing with the FP or pinching off of it. (F) This image shows the membrane separation from the box in E at higher magnification, with the two arrows identifying two different separations (yellow arrow, the broader FP separation; blue arrow, the tighter apposition found in mature GJs). Calibration bars, 0.1 μm.

indicative of reduced separation (Supplemental Figure S2). Large, highly prominent pits on the E-face (Figure 3D) could conceivably represent dimples left by a single pair of docked particles; pits from these 10-nm particles would lie at the bottom of the dimple. If this is correct, particle aggregation would then follow docking, possibly very close in time due to biophysical considerations (Braun *et al.*, 1984).

Role of the C-terminus of Cx43 in the process of GJ assembly

Because the C-terminus is a critical regulatory region in Cx43 (Ek-Vitorin *et al.*, 1996; Sorgen *et al.*, 2004; Solan and Lampe, 2009) and the major region engaged in binding different partner proteins (Laird, 2010), it can be envisioned as playing a key role in executing and regulating GJ assembly. In previous electrophysiological studies (Maass *et al.*, 2007), it was shown that a truncation mutant of Cx43 (M257) lacking residues 258–383 can assemble into a smaller number of functional GJ channels. Other, dye transfer studies raised the possibility of a reduced rate or efficiency of assembly (TenBroek *et al.*, 2001). Immunolocalization studies also revealed reduced numbers of GJs with the truncation (Maass *et al.*, 2007). However, it was not known whether or how the deletion specifically affects FP structure, either qualitatively or quantitatively, during the assembly process. Thus we next sought to determine with FF methods and EM how development of the FP is affected by deleting the C-terminus of Cx43.

We began with N2A cells transfected with Cx43 or with M257 in order to build on our earlier dye transfer studies (TenBroek *et al.*, 2001). We chose a single assembly time (3 h) for the initial analysis, reasoning that this would allow the M257 cells ample time to assemble GJs, even if more slowly. Our results are summarized quantitatively in Table 2, which shows the full spectrum of junctional structures in the Cx43 transfectants, but, surprisingly, no FPs and only three GJs in the M257 sample. This meant that the N2A system, although useful for qualitative analysis of the Cx43 transfectants (see earlier discussion and Figure 3), was unsatisfactory for a detailed quantitative comparison of the Cx43 and M257 cells.

Thus we switched to HeLa cells transfected with either Cx43 or M257, to continue our comparative studies. The two transfectants showed similar qualitative features of FP and GJ development. Plaques without aggregates, termed FP(–)s (Figure 4, A and B), and those with aggregates, termed FP(+)s (Figure 4, C and D), were found in both cell lines. Nearly mature GJs were also observed

	Cx43	M257
Initiation		
Total number of FPs plus mature GJs	47	3
Plaque area/FP (geometric mean, μm^2)	0.49 (SEM 0.37–0.63)	0
Maturation		
Number of FPs (with countable particles or pits)[a] + mature GJs	40 (100%)	3 (100%)
Number (%)[b] of FP(−)s	1 (2.5%)	0 (0%)
Number (%) of FP(+)s	26 (65%)	0 (0%)
Number (%) of mature GJs	13 (32.5%)	3 (100%)
Plaque area/GJ (geometric mean, μm^2)	0.008 (SEM 0.006–0.01)	0.006 (SEM 0.003–0.012)
Growth		
Unaggregated particles/FP (geometric mean)	160 (SEM 118–215)	0
Aggregated particles/FP(+) (geometric mean)	146 (SEM 111–192)	0
Total particles/FP (geometric mean)	354 (SEM 270–463)	0
Aggregated particles/GJ	56 (SEM 43–74)	36 (SEM 23–57)

N2A cells stably transfected with full-length Cx43 or truncated M257 were dissociated, recovered, and then reaggregated for 3 h. All samples were processed for routine freeze-fracture analysis. Comparable numbers of replicas were studied for a similar time on the EM for each different sample. Substantial assembly was detected with full-length Cx43 but very little with M257, as documented here. The data are based on four different experiments each, with multiple samples.

[a]Only these FPs were used for data derived from particle counts.

[b][Number/total (FP(±)s plus mature GJs)] × 100, using only FPs with countable particles and/or pits.

TABLE 2: Freeze-fracture EM analysis of reaggregated N2A cells expressing Cx43 or M257.

(Figure 4E; just Cx43 is shown). The general appearance of the FPs, with flat plasma membrane regions, a paucity of smaller particles, and variable number of the 10-nm particles, was similar in the two systems. Both cell types showed variations in the reduction of intermembrane distances within FPs (Figure 4F for Cx43; M257 not shown), as described here earlier for N2A cells.

However, images such as Figure 4G suggested that recruitment of 10-nm particles was impaired in the M257 cells. (Similar images were not found with HeLa-Cx43 cells.) On the basis of such images and the suggestions from earlier studies that the C-terminal (CT) truncation might decrease the efficiency of assembly, we reasoned that quantitative analysis of FP development by the two transfectants might uncover additional differences that could implicate the CT tail in specific phases of assembly.

Thus we next undertook a detailed quantitative study of FPs and GJs in FF samples of HeLa Cx43 and M257 transfectants assembled for three different time periods. We organized the data in Table 3 according to the three different phases of GJ assembly in our model: initiation, maturation, and growth (Johnson *et al.*, 2002).

Initiation of assembly. The most obvious measure of initiation is the total number of FPs and mature GJs seen at the end of an assembly period. As shown in Table 3, the total gradually decreases with time for the Cx43 cells, suggesting a possible net loss of some FPs (chiefly FP(–)s) between 1 and 6 h; the total increases with time for the M257 cells. The total for the Cx43 cells is greater at all times (15× at 1 h, 4× at 3–3.5 h, and 1.7× at 6 h). These results suggest that FP initiation by the M257 cells is delayed, with the large discrepancy fading by 6 h; connexin expression levels may also contribute.

Another measure of initiation is the mean area of observed FPs, presumably reflecting the extent of recruitment of lipids to the plaques, along with any proteins that might underlie the newly differentiated plaque membranes, as well as the loss of nonplaque components. The mean area per FP was not significantly different between the Cx43 and M257 cells at either of the first two time points ($p = 0.92$ at 1 h and $p = 0.96$ at 3–3.5 h) but was greater for the M257 at 6 h ($p < 0.0009$). The lack of a difference at 1 and 3–3.5 h is consistent with the general qualitative similarities described here earlier for the two transfectants. The significant difference at 6 h is unexplained.

Maturation during assembly. The aggregation of 10-nm particles, a distinctive feature of GJ assembly, is central to the maturation phase. According to our model, FP(–)s initially develop without aggregates, they mature as aggregates appear (FP(+)s), and, as further aggregation ensues, they eventually develop into mature GJs. Thus the extent of maturation should be reflected in the proportions of the three junctional forms (shown graphically in Figure 5, A and B) and in the number of aggregates/FP (see Table 3, Maturation). By both measures, at 1 h of cell reaggregation, maturation has apparently occurred faster in the Cx43 cells than in the M257 cells, that is, in the Cx43 cells the percentage of FP(+)s and GJs is greater (64 vs. 25%) and, of most significance, there were many more aggregates (49 vs. only 1). By 3–3.5 h, although there remained four times as many FPs plus GJs in the full-length transfectants as with the truncation, the percentages with FP(+)s and GJs were similar, and the number of aggregates per FP(+) was comparable (1.31 vs. 1.57, respectively; not significantly different, $p = 0.6$). After 6 h of reaggregation, the total number of FPs plus mature GJs was higher in the full-length samples (24 vs. 14), but the number of aggregates (including mature GJs) was comparable in the two samples, that is, 34 for full length versus 33 for M257. However, cells expressing full-length Cx43 had 25% fewer total aggregates (including GJs) than seen at 3 h (consistent with aggregate fusion over time), whereas the M257 cells had more than double the number of aggregates (including mature GJs) from 3 to 6 h. Finally, there was not a significant difference in the areas of mature GJs at 6 h between the Cx43 and M257 cells ($p = 0.06$).

Thus there are two observations that seem hard to reconcile. First, in cells expressing the truncated form, there appeared to be a delay in the development of FP(+)s and GJs continuing even to 6 h. Second, however, the actual process of particle aggregation, which was initially delayed, appeared to accelerate between 3 and 6 h of assembly. This might all be explained by a slower rate of accumulation of particles in FPs in the M257 cells, along with an enhanced aggregation of the particles that do accumulate. This interpretation is consistent with differences seen in the densities of unaggregated particles in FPs from the two different transfectants

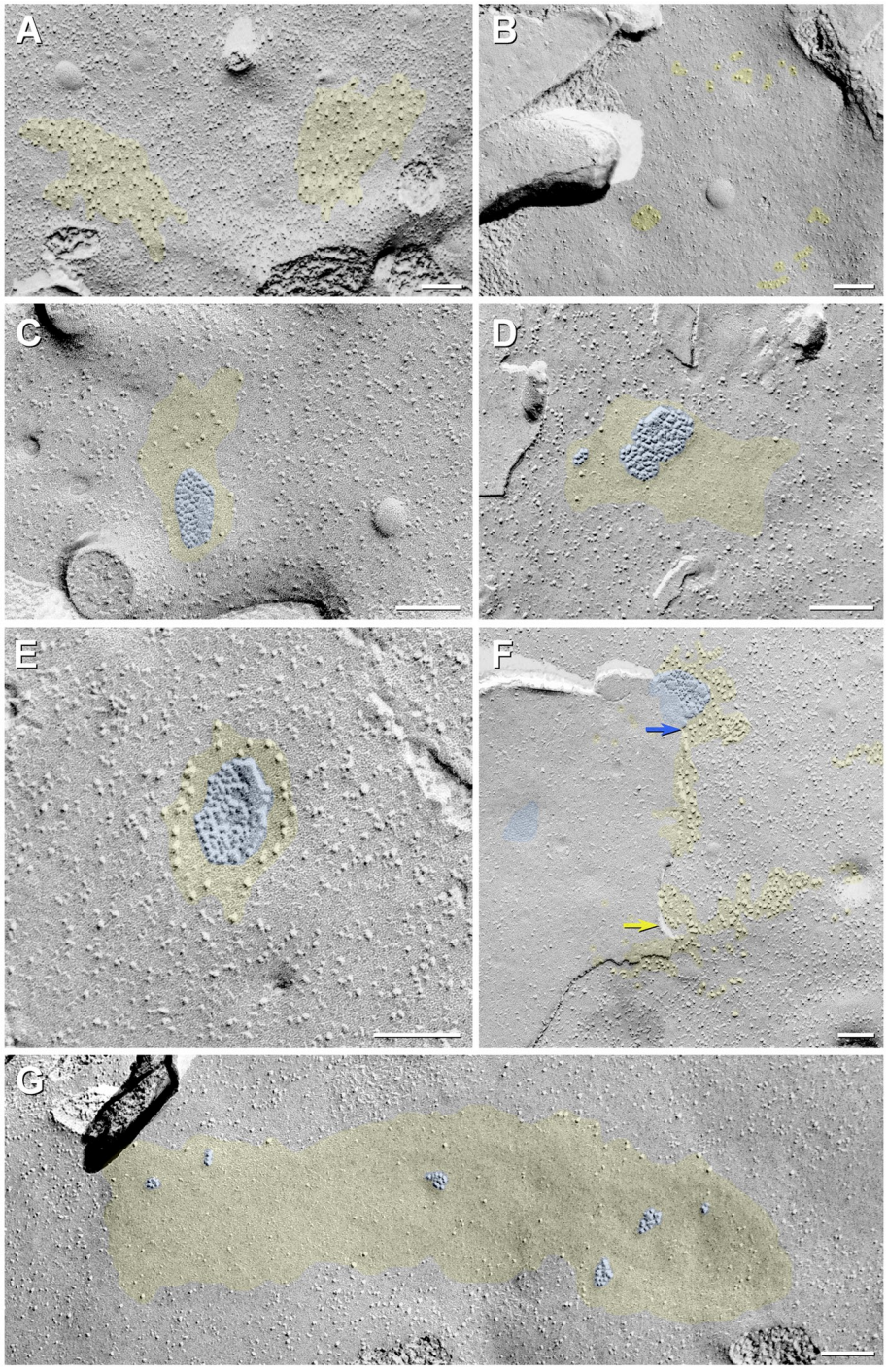

FIGURE 4: Images from FF replicas of HeLa cells, expressing either full-length Cx43 (clone Cx43-F) or the truncation mutant (clone M257-2.2), reaggregated for 1–3 h. (A) Two FPs (yellow overlays) without particle aggregates in HeLa-Cx43-cells. (B) Possible small FPs (yellow overlays) without particle aggregates in HeLa-M257-cells, particularly in the lower right corner, all containing very few unaggregated particles. Moderately sized FP(+)s (yellow overlays) with particle aggregates (blue overlays), in HeLa-Cx43-cells (C) or HeLa-M257-cells (D). (E) Modest, hexagonally packed GJ (blue overlay) in cells expressing full-length Cx43, with a ring of unaggregated particles (yellow overlay) surrounding it. (F) Fracture face skips from one FP membrane to another in the middle of the plaque from HeLa-Cx43 cells. Different intermembrane separations are shown: 1) highly irregular cell apposition outside the FP (upper left), 2) closely apposed membranes, but still exceeding 10 nm (yellow arrow), and 3) a reduced separation as found in mature GJs (blue arrow). (G) Large FP (measuring ~1.3 μm in length, yellow overlay) strikingly devoid of unaggregated particles in this HeLa-M257 cell. Several small aggregates (blue overlays) are present. Calibration bars, 0.1 μm.

(Table 3, Maturation). That is, the average densities of unaggregated particles in FP(+)s at 1, 3, and 6 h for the Cx43 cells (606, 480, and 559 respectively) are significantly higher than those for the M257 cells at those times (117, 151, and 180). Lower connexin levels in M257 cells could contribute to the slower rate of accumulation but not to the different densities of unaggregated particles. If densities of unaggregated particles are considered measures of the "concentration" of particles required to initiate aggregation (Johnson *et al.*, 1974; Preus *et al.*, 1981b), then it appears that particle aggregation can occur more readily, that is, at a lower concentration of unaggregated particles, in the M257 than in the Cx43 cells. Note that the densities of unaggregated particles in the FP(−)s are higher than those for FP(+)s, a possible reflection of a "supersaturation" effect reported earlier for FPs in Novikoff cells (Preus *et al.*, 1981b).

Our analysis of GJ aggregates and maturation in reaggregating cells also revealed three novel and significant findings on a new parameter—packing density in aggregates. First, in cells expressing full-length Cx43 the densities of particle packing in aggregates were found to increase significantly with reaggregation time (Table 3), from a mean of 6569 particles/μm^2 at 1 h to 8952 particles/μm^2 at 6 h (with $p < 0.0005$). Particle densities for Cx43 at 1 h are also different from those at 3 h ($p < 0.007$), and those at 3 h are different from those at 6 h ($p < 0.05$).

Second, we found that cells expressing the truncated connexin M257 failed to exhibit the same progressive increases in packing density with reaggregation time seen in Cx43 cells; for example, there was no increase from 3 to 6 h ($p = 0.57$). As a result, M257 cells displayed significantly lower particle densities at 6 h than did Cx43 cells ($p < 0.05$), with means of 7576 and 8952 particles/μm^2, respectively. This indicates that the packing of 10-nm particles is impaired with the truncation.

Third, *within* individual FPs, the particle packing densities of aggregates were more uniform than expected from the variation of mean densities *among* FPs from the same assembly sample. (See Supplemental Table S1 and Supplemental Figure S3 for regression analysis and determination of SD/mean.) Cx43 FPs exhibited this uniformity more than M257 FPs. These results suggest that for the Cx43 cells, and less often for the M257 cells, the packing density is somehow "coordinated" among aggregates within an FP. N2A-Cx43 cells also showed the same

	Cx43 cells			M257 cells		
	1 h	3–3.5 h	6 h	1 h	3–3.5 h	6 h
Initiation						
Total number (%) of FPs plus mature GJ	64 (100%)	36 (100%)	24 (100%)	4 (100%)	9 (100%)	14 (100%)
Plaque area/FP (geometric mean, in μm^2, with SEM)	0.054 0.049–0.059	0.061 0.054–0.070	0.067 0.054–0.081	0.052 0.042–0.063	0.060 0.035–0.105	0.144 0.095–0.218
Maturation						
Number (%) of FP(−)s	23 (36%)	3 (8%)	0 (0%)	3 (75%)	0 (0%)	0 (0%)
Number (%) of FP(+)	39 (61%)	26 (72%)	13 (54%)	1 (25%)	7 (78%)	9 (64%)
Number (%) of mature GJs	2 (3%)	7 (19%)	11 (46%)	0 (0%)	2 (22%)	5 (36%)
Total number of aggregates in FP(+)s	49	38	23	1	11	28
Area/mature GJ (μm^2, geometric mean, with SEM)	0.068 0.042–0.110	0.008 0.006–0.011	0.013 0.011–0.021	NA 0	0.013 0.005–0.035	0.005 0.004–0.006
Packing density of aggregated particles in FP(+)s (geometric mean, per μm^2, SEM)	6569 6225–6933	7780 7743–8131	8952 8595–9324	5574 NA	7288 6972–7618	7577 7109–8074
Density of unaggregated particles/FP(−) (geometric mean, per μm^2, SEM)	904 823–993	1051 719–1537	NA NA	375 366–384	NA NA	NA NA
Density of unaggregated particles/FP(+) (geometric mean, per μm^2, SEM)	606 558–659	480 422–546	559 489–639	117 NA	150 110–205	181 141–234
Growth						
Unaggregated particles/FP (geometric mean, SEM)	37 34–41	32 26–38	37 30–47	14 9–23	9 7–12	26 21–33
Aggregated particles/FP(+) (geometric mean, SEM)	38 32–46	79 64–99	69 54–89	35 NA[b]	36 28–47	103 (78)[a] 74–144
Total particles/FP (geometric mean, SEM)	63 56–70	119 100–142	114 92–142	26 21–32	49 39–61	138 (108)[a] 103–185
Total particles/mature GJ (geometric mean, SEM)	446 330–603	70 49–99	107 81–141	NA NA	81 48–117	49 39–62
Total particles/(FPs plus GJs) (geometric mean, SEM)	67 60–75	107 92–125	111 94–131	26 21–32	55 43–70	95 (80)[a] 75–122

See *Materials and Methods* for details related to EM sampling. The three GJ assembly parameters evaluated here are described in the *Results* section. Because the values for the areas of FPs and mature GJs, the numbers of particles found within them, and densities are skewed, the mean values for these features are expressed as geometric means (see *Materials and Methods*). Statistical values derived from *t* tests for various parameters are found in the *Results* section.

[a]In these samples, there were small numbers of FP(+)s, including one large outlier in each case. When this value is not included, the geometric mean for the sample is shown in parenthesis.

[b]Only one FP(+) in this sample.

TABLE 3: Freeze-fracture EM analysis of HeLa cells in an assembly assay versus reaggregation time.

phenomenon, although they were studied only at one time point (data not shown).

Thus the packing parameter appears to provide a quantitative measure of a previously unrecognized maturation process, which is dependent on or affected by the CT tail. The changes in particle packing within aggregates could depend on interactions between connexin hemichannels and/or between Cx43 and its binding partners. The data are consistent with a model in which low-density aggregates form first, perhaps based on a biophysical mechanism for GJ stability (Braun *et al.*, 1984). Aggregation of this type is found in both the Cx43 and M257 cells. Subsequently, interacting proteins, including scaffolding proteins like ZO-1 (Hunter *et al.*, 2005), could link connexins laterally to produce high-density aggregates. Aggregation of this second type appears to be defective in M257 cells.

Growth during assembly. We examined the number of 10-nm particles in order to focus on the recruitment of Cx43 to developing FPs (Table 3, Growth). It was clear that recruitment was well developed in the Cx43 cells over the initial 3 h but had begun to plateau by 6 h. Total number of 10-nm particles/FP (including mature GJs) at 3 h was almost twice that at 1 h (significantly different, $p < 0.02$) but did not increase significantly at 6 h. However, recruitment in M257 cells over the 6-h time period did not match that in the full-length cells. Cx43 cells had nearly twice as many total particles/FP at 1 and 3 h than the M257 cells, ($p < 0.04$ and $p < 0.05$, respectively) but no significance difference at 6 h. Of interest, unlike the Cx43 cells, the M257 cells did show an increase in the total number of 10-nm particles/FP from 3 to 6 h, indicating that recruitment had continued. This comparison over time of total particles in both FPs and mature GJs is found in Table 3 and shown in histogram form in Figure 5C.

The quantitative EM analysis of GJ assembly revealed several novel things about GJ formation between cells lacking the C-terminus of Cx43, in different phases of assembly. Two aspects of particle aggregation, part of the maturation process, were found to be altered with connexin truncation: 1) initial aggregation occurred at a lower "concentration" in FPs and 2) the high-density packing found

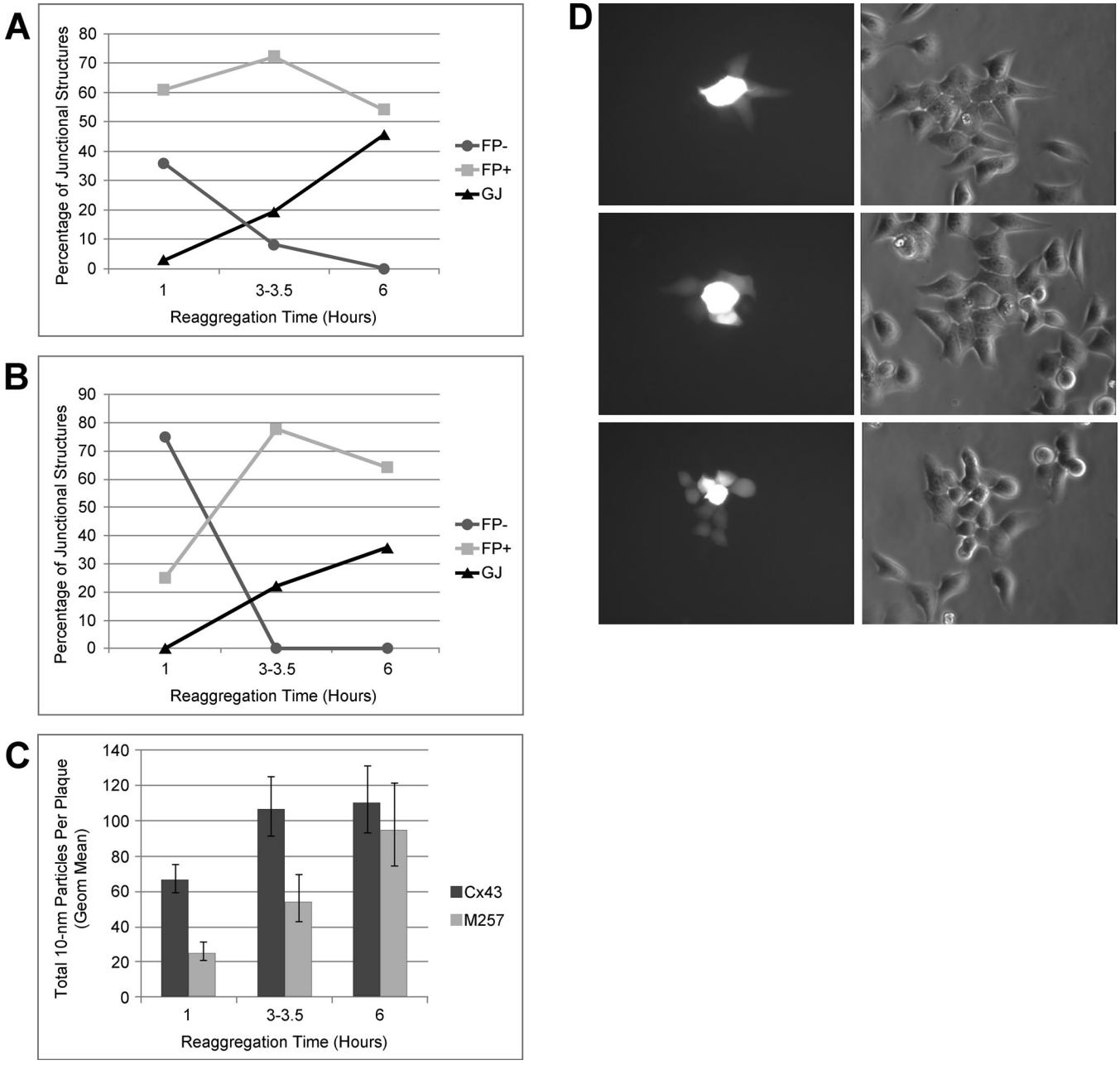

FIGURE 5: Analysis of GJ assembly in stable transfectants expressing either full-length Cx43 or M257. For HeLa-Cx43-F cells (A) or the M257 truncation (B), percentages of the three classes of junctional structures (FPs without aggregates, FPs with aggregates, and mature GJs, as noted) are plotted vs. reaggregation time. (C) Histogram summarizes differences between the two lines in terms of total 10-nm particles displayed on a per plaque basis vs. reaggregation time; includes both FPs and mature GJs. Error bars are asymmetrical for geometric means (see *Materials and Methods*). (D) Examples are given of results from Lucifer yellow injection experiments following reaggregation with M257-2.2 cells. Calibration bar, 15 μm.

with full-length Cx43 was lacking. There were also significant effects on growth, which could be attributed to truncation effects and/or expression levels in the two lines. However, what is striking is that the areas of developing FPs, a measure of initiation, were not affected, in spite of reduced numbers of 10-nm particles at 1 and 3 h.

Role of the C-terminus of Cx43 in the inhibition of GJ assembly by PKC

Here we used dye transfer to determine whether the C-terminus of Cx43 is also required for the dramatic inhibition of assembly seen following PKC activation (Lampe, 1994). Results of dye injection experiments on reaggregated HeLa-M257 cells are shown in Figure 5D. When HeLa cells (three clones) expressing full-length Cx43 were treated with TPA to activate PKC immediately prior to and during reaggregation in 1 h GJ assembly assays, the development of dye transfer was completely inhibited (Figure 6A), regardless of the baseline level of communication. Because established cultures of the HeLa-Cx43-K clone maintained significant communication for at least 1 h following TPA treatment (Supplemental Figure S4A), the TPA inhibition of assembly by this clone was

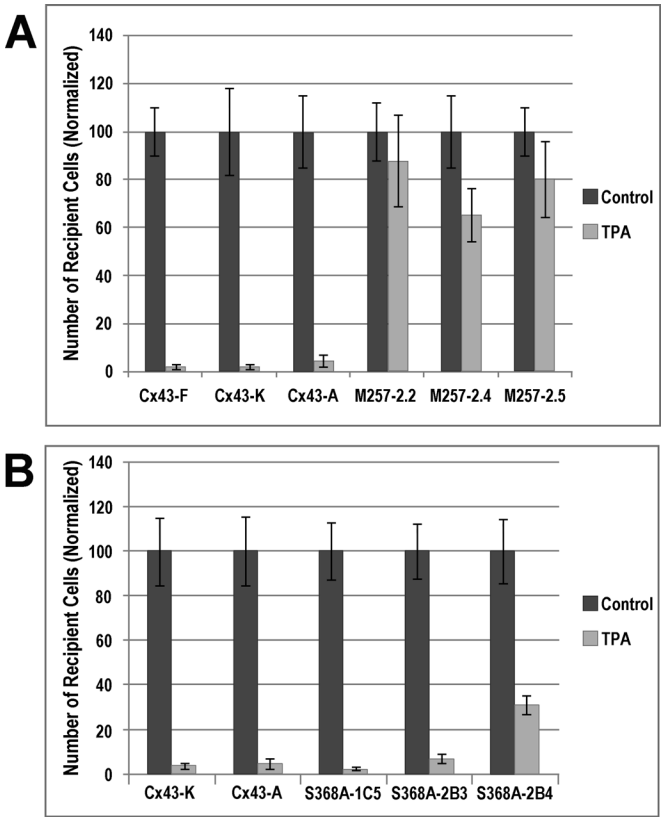

FIGURE 6: Regulation of GJ assembly following the activation of PKC in reaggregated transfectants expressing C-terminal mutations in Cx43. Effects of TPA on dye transfer are shown as normalized values, with control values for each clone being set at 100%. (A) Effects of M257 truncation were determined by comparison of dye transfer with cells expressing full-length Cx43. Multiple clones are shown for both transfectant types. TPA suppresses communication between cells of the three full-length clones ($p < 0.0001$) but not between those lacking the C-terminus ($p = 0.59$, 0.06, and 0.39). (B) Mutagenesis of Ser-368 to alanine and analysis of GJ assembly in different cell clones, compared with others expressing wild-type Cx43. Two clones with the Ser368Ala mutation displayed nearly complete inhibition of communication following activation of PKC by TPA, despite the mutation, whereas the other showed ~70% inhibition. Dye transfer was significantly inhibited in all six lines ($p < 0.0001$). Thus phosphorylation of Ser-368 is not essential for complete inhibition. The number of dye-injected cells for each cell line averages ~20 for the control and also for TPA, with the totals in both A and B averaging 200.

independent of a gating effect. Inhibition of the other two Cx43 clones possibly involved some gating. These results parallel those previously reported with Novikoff cells (Lampe, 1994), for which TPA inhibited the development of dye-permeable pathways and also the assembly of FPs between reaggregated cells. It is striking, however, the TPA-induced inhibition of communication was largely prevented by truncation of Cx43 at position 257 (Figure 6A), a result observed in all three clones. These experiments demonstrate that the C-terminus of Cx43 is critical for the inhibition of GJ assembly by PKC. The findings parallel our previous report that the positive regulation of GJ assembly involving Cx43, which is mediated by cAMP-dependent mechanisms (Burghardt *et al.*, 1995; Wang and Rose, 1995; Paulson *et al.*, 2000), requires an intact C-terminus (TenBroek *et al.*, 2001).

Role of specific C-terminal serines in the regulation of GJ assembly

Having shown that the C-terminus of Cx43 is required for inhibition of GJ assembly by TPA, we next asked, using dye transfer, whether specific serine residues, either directly or indirectly phosphorylated following activation of PKC, play a role in this inhibitory response. We used transfectant clones that in established cultures showed no rapid TPA inhibition and thus no gating effect (e.g., Supplemental Figure S4C). Serines 255, 262, and 368 on Cx43 are known to be phosphorylated following the activation of PKC (Sirnes *et al.*, 2009; Srisakuldee *et al.*, 2009). We first evaluated the role of S368 phosphorylation in the regulation of assembly by testing stable transfectants of S368A in assembly assays (Figure 6B). As was seen with cells expressing full-length Cx43, two of these S368A transfectants showed complete inhibition of assembly by TPA (as measured with dye transfer). Because the mutation failed to block inhibition in these clones, one can conclude that phosphorylation of S368 is not required to inhibit GJ assembly following the activation of PKC. Experiments on a third clone, however, revealed that GJ assembly was inhibited, but by only ~70%, suggesting that S368 may contribute to the inhibition of assembly or that subcloning of stable transfectants may select for differing enzyme activities/isozyme profiles.

To analyze the role of other potential PKC phosphorylation sites, both an S262A site mutation and an S262A/S368A double mutation were stably transfected into HeLa cells. Assembly was analyzed in different clones, and results indicated that neither the S262A mutation nor the double mutation (S262A/S368A) significantly altered the inhibitory effect of TPA on assembly (Supplemental Figure S4, D and E); TPA continued to induce a marked inhibition in these site mutants.

Because MAP kinase can be activated by PKC (Leithe *et al.*, 2009), PKC could indirectly block assembly via Cx43 phosphorylation. However, inhibition still occurred with a triple mutant replacing serines 255, 279, and 282 (Supplemental Figure S4F), sites possibly phosphorylated by MAP kinase when activated by PKC (Warn-Cramer *et al.*, 1996). The results suggest that none of these sites, alone or in combination, is sufficient for the inhibition of assembly.

DISCUSSION

In the present study, we analyze the role of the FP in GJ assembly and identify specific regulatory functions of the Cx43 C-terminus in assembly. We demonstrate here that 1) the FP is a distinct membrane domain, characterized by 10-nm particles containing connexins, 2) the defined steps in GJ assembly involve changes both within and between membranes, including docking and particle aggregation, 3) in the absence of the C-terminal tail of Cx43, there is a delay in FP development and several aspects of particle aggregation are altered, and 4) negative regulation of GJ assembly by PKC requires the C-terminal tail.

Formation plaques are membrane domains involved in GJ assembly

Filipin labeling. There are two interpretations of the filipin labeling; both indicate that FPs are distinct membrane domains. First, FPs could have lower levels of β-hydroxysterols, most likely cholesterol, compared with surrounding membranes. This would be interesting, as different cholesterol levels have been shown to affect the activity of connexin hemichannels (Locke and Harris, 2009). Second, a protein network could underlie the FP membrane,

interfering with filipin binding, as occurs with the cholesterol-rich membranes of clathrin-coated pits or viruses (Steer *et al.*, 1984). In certain EM preparations, GJ membranes display distinctive coats on the cytoplasmic surface (Sotelo *et al.*, 1974; Sotelo and Korn, 1978; Manjunath *et al.*, 1987; De Zeeuw *et al.*, 2003). Whether FP membranes involve similar protein complexes is not known, but such specializations could also explain the stiff or rigid appearance of FP membranes. Thus proteins underlying the FP membrane (i.e., not in the bilayer), such as ZO-1 or adhesion-related proteins, could be implicated (Hunter *et al.*, 2005).

Connexin immunolabeling. A large body of FRIL data demonstrate that all mature GJs, composed of different connexins, contain membrane particles ~8–10 nm in diameter, depending on various factors (Rash and Giddings, 1989), findings consistent with analysis of isolated GJs formed by Cx43 (Unger *et al.*, 1999). Thus we know what to look for in FF replicas in terms of identifying the membrane particles (i.e., the connexons or GJ hemichannels) from which GJs will be constructed. The 10-nm particles are the only membrane particles of an appropriate size and sufficient number in the FP to represent connexin hemichannels and contribute to GJ assembly, and it is these particles that are labeled with Cx43 antibodies in the FRIL studies. Thus we have a second line of support for the idea that FPs are membrane domains, which is further strengthened by our analysis of the enrichment of 10-nm particles and the depletion of smaller particles.

When combined with the shift in junctional structures over time (Figure 5A) and the present analysis of dynamic changes within and between FP membranes, a compelling case is made for FPs serving as sites of GJ assembly, where the 10 nm particles are incorporated into GJs. An alternative interpretation—that FPs are not sites of assembly but instead sites of disassembly linked to junctional degradation—is not supported by the time-course analysis. Identifying the FP as a site of GJ assembly provides an important framework for future assembly experiments.

Membrane interactions, docking, and aggregation in formation plaques

Analysis of FP structures and dynamics during the GJ assembly process provided important support for the apparent matching of FP membranes and the progressive reduction of the intermembrane separation proposed in our assembly model. We documented that well-developed FPs involve matched membranes, seen most convincingly when P-face particle aggregates are found to be continuous with arrayed pits on an adjacent E-face. However, matching of the earliest FPs, although likely, remains uncertain. In addition, as suggested by images of relatively empty FP membranes, sparsely populated with 10-nm particles, the earliest FPs may involve few, if any, 10-nm particles.

Substantial support was also obtained for a progressive reduction of the intermembrane distance during assembly, illuminating what had been a poorly understood concept. Broad separations between membranes are clearly found in undeveloped FPs, and aggregates in FPs display intermembrane separations indistinguishable from those in GJs. The interesting question is what drives this reduction. Strong support is presented here for the role of GJ hemichannel docking in bringing membranes together, involving significant reductions of the intermembrane separation at precisely the sites of particle aggregates. Provocative images of what could be single docked particles serve to strengthen the case. The significance of this role for docking is twofold. First, it answers a long-standing question, indicating that docking occurs in the FP, in contrast to the nonjunctional membrane. Second, it would mean that docking precedes particle aggregation.

Role of the C-terminal tail of Cx43 in GJ assembly and regulation

Experiments comparing assembly with full-length Cx43 versus the truncation mutant identified several aspects by which connexin-interacting partner proteins could be envisioned to play critical roles. First, the apparent delay in assembly in M257 cells can logically be interpreted as a suppressed trafficking to the plasma membrane and/or to the FP, although we cannot rule out some contribution by lower expression levels in the M257 cells. It is possible that multiple regions within Cx43, including sequences found in M257, bind to multiple interacting proteins to facilitate recruitment to the plasma membrane and/or FP domain. Loss of the C-terminus might then affect recruitment but not exclude it. Second, the absence of high-density particle aggregates could also reflect the essential role of a binding protein that links particles together but is compromised in M257 cells. Finally, it is important to recognize that the number of unaggregated particles in M257 cells never exceeded that observed with full-length Cx43; in fact they were significantly reduced. This would support the idea that there is not an essential defect in docking and/or initial aggregation of hemichannels in the truncation mutant, because this would lead to a large excess of unaggregated particles (i.e., assembly precursors). Instead of an excess, however, the aggregation of particles in M257 cells occurred at a lower density of unaggregated FP particles than with full-length Cx43.

Other experiments demonstrated that the loss of the CT tail of Cx43 dramatically reduced the inhibition of GJ assembly mediated by PKC. These observations further emphasize the critical role of the C-terminus of Cx43 in regulating communication in a range of cell systems (Solan and Lampe, 2009) and highlight a role for kinases in modulating GJ assembly (Solan and Lampe, 2005).

Given the role of the C-terminus in regulating GJ assembly, we also sought to identify specific PKC phosphorylation sites required for the negative regulation. Five sites were evaluated. Mutating none of these sites, however, appeared to be sufficient to block the inhibition of assembly triggered by activation of PKC with TPA. The possibility remains that all three PKC sites (255, 262, and 368) must be phosphorylated for complete inhibition of assembly. Cell-specific differences in kinase profiles may also play a role in these responses. Finally, another possibility is that direct phosphorylation of Cx43 is not essential for the inhibition of assembly. Instead, an interaction could be involved between the CT tail of Cx43 and another protein affected by PKC, for example, one participating in membrane trafficking. Other studies reported PKC-mediated effects on Cx43 trafficking that occur over a time course that is consistent with the inhibition of assembly as described here (Leithe *et al.*, 2009).

MATERIALS AND METHODS

Cells

Novikoff cells, grown as reported earlier (Johnson *et al.*, 2002), were used for filipin studies. N2A cells transfected with wild-type connexin43 and M257 were kindly provided by Steve Taffet (SUNY Health Science Center, Syracuse, NY) and used for initial FF-EM studies on GJ assembly. They were maintained at 37°C in a standard incubator with 5% CO_2 in high-glucose DMEM containing 10% fetal calf serum (FCS), 100 U/ml penicillin/streptomycin, and 800 μg/ml geneticin (G418; Life Technologies, Carlsbad, CA). HeLa cells, used for FF-EM and dye injection, were kindly provided and transfected with Cx43 by Klaus Willecke (University of Bonn, Bonn, Germany; HeLa-Cx43-K) and Bonnie Warn-Cramer and Alan Lau (University of

Hawaii, Honolulu, HI; HeLa-Cx43-F, clone 4) or were generated in house via transfection (HeLa-Cx43-A), using connexin-deficient HeLa cells (American Type Culture Collection [ATCC], Manassas, VA).

For generation of clone HeLa Cx43-A, a cDNA insert containing the complete coding region of Cx43 (a generous gift from Eric Beyer, University of Chicago, Chicago, IL) was subcloned into the phagemid vector, pBluescript SK+ (Stratagene, La Jolla, CA), amplified, and then further subcloned into a pZeoSV2 vector with zeocin resistance (Invitrogen, Carlsbad, CA) for introduction into HeLa cells (ATCC). A Cx43 insert containing a stop codon at serine 257 (M257), generously donated by Mario Delmar (University of Michigan, Ann Arbor, MI), was similarly subcloned and then transferred into a pIRES expression vector (GenBank U89672) possessing hygromycin resistance. A number of stable HeLa transfectants (including HeLa-M257 clones 2.2, 2.4, and 2.5) were generated from connexin-deficient HeLa cells (ATCC) using this expression vector. These cells were maintained in low-glucose DMEM containing 10% FCS, 100 U/ml penicillin/streptomycin, and 500 µg/ml hygromycin.

Paul Lampe (Fred Hutchinson Cancer Institute, Seattle, WA) kindly donated a PIRES-puromycin resistance pcDNA construct for expression of Cx43-S368A, Cx43-S262A, and a double mutant expressing both mutations. These were used to generate stably transfected HeLa cell clones (using ATCC cells), which were maintained in low-glucose DMEM, 10% FCS, and 0.5 mg/ml puromycin. The triple MAP kinase mutants transfected into HeLa cells were kindly donated by Bonnie Warn-Cramer and Alan Lau (University of Hawaii).

The choice of cell lines and transfectant clones for the various experiments was based on the following considerations: 1) Novikoff cells, in which FPs have been characterized quantitatively in previous studies (Johnson *et al.*, 2002), were used for the filipin experiments as part of an earlier set of assembly studies only now being reported. Repeating these experiments with N2A and/or HeLa transfectants was not considered necessary, given the clear results with the Novikoff cells. 2) N2A transfectants (expressing either Cx43 or M257) were used for some of the qualitative studies and for an initial quantitative EM/FF comparison with results from our previous dye injection studies on assembly by these cells (TenBroek *et al.*, 2001). Because the Cx43-N2A cells developed very large and numerous FPs, they were especially useful in studying certain FP features, such as matching of FPs in adjacent cells, width of intermembrane separation, organization of 10 nm particles, and so on. However, the reaggregated N2A-M257 cells exhibited only a very small number of junctional structures (either FPs or GJs), making it impractical to compare the Cx43 and M257 FPs in quantitative detail. 3) HeLa cells were therefore chosen for comparing Cx43 and M257 transfectants by means of EM/FF. The HeLa-Cx43-F clone was selected, except where noted, because these cells displayed rapid assembly and allowed for sampling from numerous, actively assembling interfaces. The HeLa-M257-2.2 clone was chosen for comparison because, based on dye transfer, it was representative of several clones expressing the Cx43 truncation. However, the Cx43-K clone was the primary "control" for the dye injection studies of TPA-induced inhibition of assembly. In contrast to the Cx43-F clone (results not shown), the Cx43-K clone in established cultures continued to display substantial communication after 75 min in the presence of TPA (Supplemental Figure S4A), that is, only partial inhibition of permeability (gating), and thus provided the most unambiguous comparison with TPA effects on assembly by the M257 transfectants and CT site mutants.

Assembly protocol

Novikoff cells were reaggregated according to established methods (Johnson *et al.*, 2002). Both N2A and HeLa cells were passaged 2 d prior to an experiment, and a change of fresh medium occurred 24 h prior to the experiment. To achieve complete confluence following assembly, 100-mm dishes of cells at 80–100% confluency were dissociated and then reassembled in 35-mm culture dishes. Cells were dissociated with 1 ml of 0.25% trypsin-EDTA (Life Technologies) for 1.5 min at 37°C, the trypsin neutralized with complete DMEM medium containing FCS, and the cell suspension centrifuged to remove the neutralized trypsin. Cells were then gently resuspended in fresh medium containing 12.5 mM 4-(2-hydroxyethyl)-1-piperazineethanesulfonic acid buffer and transferred to adhesion-blocked poly-2-hydroxyethyl methacrylate–coated centrifuge tubes for a recovery period of 90 min on a shaker platform in a 37°C incubator with rotation at 200 rpm. During this period, cells internalize disrupted GJs from the cell surface (Preus *et al.*, 1981a). The suspension was passed through a sterile 35-µm filter to remove any large clumps of cells. The final cell preparation was plated onto 35-mm dishes by gentle centrifugation at 750 rpm for 10 min. Cell reaggregation and subsequent assembly of junctions was allowed to proceed by placing the dishes in a standard CO_2 incubator at 37°C for 3 h in the case of N2A cells and for 1–1.5 h with HeLa cells. For the time-course evaluation of GJ assembly in HeLa cells with FF-EM, at least two experiments were evaluated for each of the two samples (full-length and truncated Cx43) at each time point.

Fixation

For filipin-labeling studies, Novikoff cells were prefixed for 15 min in 2% glutaraldehyde, 0.05% $CaCl_2$, and 1% dimethylsulfoxide in a 0.1 M sodium cacodylate buffer (Johnson *et al.*, 2002). Then control samples were treated with fresh fixative of the same type, typically for 3 h at 25°C. Experimental samples were treated with the control fixative to which had been added 300 µM filipin (Upjohn, Kalamazoo, MI). For conventional FF work, assembled monolayers of N2A or HeLa cells were rinsed with Hank's buffered saline containing calcium and magnesium and were then fixed in 2% glutaraldehyde in 0.1 M sodium cacodylate buffer overnight at 4°C. For FRIL studies, cells were fixed for 1 h in 4% formaldehyde in 0.15 M Sorenson's phosphate buffer at pH 7.4.

Sample freezing

For the conventional freeze-fracturing and for the filipin work, after three washes in 0.1 M cacodylate buffer to remove fixative, the cell cultures were scraped with a rubber policeman and transferred to a 1.6-ml Eppendorf tube. Following short centrifugations to produce loose pellets of cells, the supernatants were removed and replaced with fresh cacodylate buffer containing 20% glycerol cryoprotectant, and this was allowed to infiltrate for 1–2 h at room temperature. Samples were briefly centrifuged, transferred to gold FF "hats," and then frozen by plunging into liquid propane cooled to −190°C and stored in liquid nitrogen until fracturing. For FRIL, samples were cryoprotected with 30% glycerol and plunge-frozen into liquid propane/ethane cooled with liquid nitrogen.

Fracturing

For the filipin studies and for the conventional freeze-fracturing, samples were fractured in a Balzers BAF 060 FF apparatus (Bal-Tec; now Leica Microsystems, Buffalo Grove, IL). They were shadowed with a platinum/carbon source at a 45° angle and then carbon coated. For FRIL studies, samples were fractured in a JEOL 9010c freeze-fracture machine (RMC/Boeckler; JEOL, Akishima, Japan), rotary coated with 1 nm of carbon, and unidirectionally shadowed (60°) with 1.0–1.5 nm of platinum/carbon, followed by 20 nm of carbon (Rash

et al., 1998, 2004b; Rash and Yasumura, 1999; Kamasawa *et al.*, 2006). A gold index grid containing a droplet of 1.5–2.5% Lexan plastic dissolved in dichloroethane was placed on the frozen surface of the replica, and the solvent was evaporated at 35 to 20°C.

Replicas

For standard FF, individual samples in their gold holders were allowed to thaw at room temperature prior to floating the replica onto a freshly prepared solution of 25% bleach. After 1 h of digestion to remove the adherent tissue, the replicas were washed in distilled water. For FRIL studies, replicas were washed for ~29 h at 48–50°C in 2.5% SDS detergent and rinsed for 30–90 min in blocking buffer, which consists of 1.5% fish gelatin digest and 10% heat-inactivated goat serum (both from Sigma-Aldrich, St. Louis, MO) in Sorenson's phosphate buffer (Rash and Giddings, 1989). Replicas were then immunolabeled in blocking buffer (Fujimoto, 1995; Rash and Yasumura, 1999; Furman *et al.*, 2003), using affinity-purified antibodies to mouse anti-Cx43 (MAB3068; Chemicon, Millipore, Billerica, MA). Goat anti–mouse immunoglobulin G conjugated to 5-, 10-, and 20-nm gold beads was from BB International (Ted Pella, Redding, CA). Labeled replicas were rinsed in distilled water and air dried at 60°C, and a stabilizing 20-nm coat of carbon was applied to the labeled side of the replica. The Lexan support film was removed by immersion of the labeled replicas in dichloroethane for 6–9 h.

Electron microscopy

Conventional replicas were examined in several different microscopes. Each grid was scanned in a consistent pattern and all apparent membrane surfaces closely scrutinized. Any junctional components encountered were photographed routinely on film at a magnification of 30,000, and areas of special interest at 50,000. For FRIL analysis, replicas were examined at 100 kV in a JEOL 2000 EX-II TEM equipped with a 60° tilting (goniometer) stage or in a JEOL 1200 EX TEM equipped with a 45° tilting stage. Selected areas were photographed as stereoscopic pairs having an 8° included angle, and all images were analyzed stereoscopically. Despite their low electron opacity, 5-nm gold beads were especially useful because they typically label at two to eight times the labeling efficiency of progressively larger gold beads (10 and 20 nm) and hence may be used for semiquantitative analysis of connexins (Rash and Yasumura, 1999; Rash *et al.*, 2004a). Stereoscopic viewing was essential for determining whether gold beads were on the tissue side of the replicas (potentially specific labeling) versus on the Lexan coated side, that is, necessarily nonspecific labeling (Rash and Yasumura, 1999).

In the quantitative analysis of GJ assembly by N2A and HeLa transfectants, we found that areas of membrane apposition between adjacent cells were somewhat irregular immediately following contact. Thus we did not find large membrane fractures that represented entire interfaces between cells as had been found between the Novikoff cells studied previously (Johnson *et al.*, 2002). Because this precluded an analysis of GJ assembly on a cell interface basis, we instead examined all membrane fractures (large and small) in each of the various samples, that is, both control and experimental cells at all reaggregation time points, studying each sample on the EM for a comparable period of time. With fewer FPs observed in M257 cells (and less time spent collecting images), actual observation time was greater for these cells. This approach provided for collection of a strong data set describing the properties of developing FPs and GJs with and without the truncation of Cx43. With the approach, the number of junctional structures is a less reliable parameter and is also affected by connexin expression levels. For these assembly experiments, individual FP parameters and all 10-nm particles were enumerated (Johnson *et al.*, 2002), as well as the areas and particle numbers for the mature GJs.

Following the analysis of the assembly experiments, images were scanned (Umax MagicScan), transferred to a computer, and subsequently examined and analyzed with Image Pro, version 4.0 (Media Cybernetics, Bethesda, MD), software. Magnifications were confirmed by calibrating the microscope using a standard diffraction grating replica (Ernest F. Fullam, Ted Pella), and measurements were then converted to pixels for data collection and comparison. FRIL negatives were scanned and digitized using an ArtixScan 2500f digital scanner (Microtek, Carson, CA) and processed using Photoshop CS2 (Adobe Systems, San Jose, CA).

Dye injection

Injection of Lucifer yellow into various HeLa transfectants was used to monitor GJ communication between cells as reported previously (TenBroek *et al.*, 2001) by assaying for the number of recipient cells detected 5 min after injection (or as noted in the figure legends). In most cases, recipient cells were counted by eye at the 5-min point, although digital images were collected in some later experiments. Parental HeLa cells used for the transfections displayed little to no dye transfer (based on three experiments; data not shown); the occasional limited transfer was presumably due to a low level of expression of a native connexin. For the studies of the effect of TPA on assembly, TPA was present during the last 15 min of the recovery period and throughout the assembly period. The average number of cells receiving dye with TPA was normalized to the average number of cells receiving dye in the untreated cells.

Statistical analysis

For the GJ assembly analysis, since it has been shown that the developing FPs and GJs exhibit a skewed distribution (Preus *et al.*, 1981b), the data on particle numbers and FP areas were presented as geometric means, and standard errors were determined. The latter values, which incidentally are not symmetrical, were then back-transformed for presentation in the tables. Statistical significance was determined by *t* tests on the transformed data, with $p < 0.05$ considered significant. For the dye injection experiments, numbers of recipient cells were expressed as arithmetic means ± SEM and evaluated with *t* tests; $p < 0.05$ was considered significant. For presentation of dye transfer data, samples treated with TPA were normalized to the untreated controls.

ACKNOWLEDGMENTS

We are grateful to James Nagy and Alberto Pereda for fruitful discussions related to the manuscript, to Mario Delmar and Steve Taffet for N2A cells, to Klaus Willecke for HeLa cells expressing Cx43, to Alan Lau and Bonnie Warn-Cramer for cells expressing the MAP kinase mutations, and to Paul Lampe for constructs. The work was supported by National Institutes of Health Grant GM-46277 to R.G.J. and J.D.S. and by National Institutes of Health Grant NS-44395 to J.E.R.

REFERENCES

Beardslee MA, Laing JG, Beyer EC, Saffitz JE (1998). Rapid turnover of connexin43 in the adult rat heart. Circ Res 83, 629–635.

Beyer EC, Gemel J, Martinez A, Berthoud VM, Valiunas V, Moreno AP, Brink PR (2001). Heteromeric mixing of connexins: compatibility of partners and functional consequences. Cell Commun Adhes 8, 199–204.

Biswas SK, Lo WK (2007). Gap junctions contain different amounts of cholesterol which undergo unique sequestering processes during fiber cell differentiation in the embryonic chicken lens. Mol Vis 13, 345–359.
Braun J, Abney JR, Owicki JC (1984). How a gap junction maintains its structure. Nature 310, 316–318.
Burghardt RC, Barhoumi R, Sewall TC, Bowen JA (1995). Cyclic AMP induces rapid increases in gap junction permeability and changes in the cellular distribution of connexin43. J Membrane Biol 148, 243–253.
Burt JM, Steele TD (2003). Selective effect of PDGF on connexin43 versus connexin40 comprised gap junction channels. Cell Commun Adhes 10, 287–291.
Cooper CD, Lampe PD (2002). Casein kinase 1 regulates connexin-43 gap junction assembly. J Biol Chem 277, 44962–44968.
Cronier L, Crespin S, Strale PO, Defamie N, Mesnil M (2009). Gap junctions and cancer: new functions for an old story. Antioxid Redox Signal 11, 323–338.
De Zeeuw CI *et al.* (2003). Deformation of network connectivity in the inferior olive of connexin 36-deficient mice is compensated by morphological and electrophysiological changes at the single neuron level. J Neurosci 23, 4700–4711.
Decker RS, Friend DS (1974). Assembly of gap junctions during amphibian neurulation. J Cell Biol 62, 32–41.
Dobrowolski R, Willecke K (2009). Connexin-caused genetic diseases and corresponding mouse models. Antioxid Redox Signal 11, 283–295.
Ek-Vitorin JF, Calero G, Morley GE, Coombs W, Taffet SM, Delmar M (1996). PH regulation of connexin43: molecular analysis of the gating particle. Biophys J 71, 1273–1284.
Elias PM, Friend DS, Goerke J (1979). Membrane sterol heterogeneity. Freeze-fracture detection with saponins and filipin. J Histochem Cytochem 27, 1247–1260.
Fallon R, Goodenough DA (1981). Five-hour half-life of mouse liver gap junction protein. J Cell Biol 90, 521–526.
Fujimoto K (1995). Freeze-fracture replica electron microscopy combined with SDS digestion for cytochemical labeling of integral membrane proteins. Application to the immunogold labeling of intercellular junctional complexes. J Cell Sci 108, 3443–3449.
Fujimoto K, Nagafuchi A, Tsukita S, Kuraoka A, Ohokuma A, Shibata Y (1997). Dynamics of connexins, E-cadherin and alpha-catenin on cell membranes during gap junction formation. J Cell Sci 110, 311–322.
Furman CS, Gorelick-Feldman DA, Davidson KG, Yasumura T, Neely JD, Agre P, Rash JE (2003). Aquaporin-4 square array assembly: opposing actions of M1 and M23 isoforms. Proc Natl Acad Sci USA 100, 13609–13614.
Gaietta G, Deerinck TJ, Adams SR, Bouwer J, Tour O, Laird DW, Sosinsky GE, Tsien RY, Ellisman MH (2002). Multicolor and electron microscopic imaging of connexin trafficking. Science 296, 503–507.
Henderson D, Eibl H, Weber K (1979). Structure and biochemistry of mouse hepatic gap junctions. J Mol Biol 132, 193–218.
Hunter AW, Barker RJ, Zhu C, Gourdie RG (2005). Zonula occludens-1 alters connexin43 gap junction size and organization by influencing channel accretion. Mol Biol Cell 16, 5686–5698.
Johnson R, Hammer M, Sheridan J, Revel JP (1974). Gap junction formation between reaggregating Novikoff hepatoma cells. Proc Natl Acad Sci USA 71, 4536–4540.
Johnson RG, Meyer RA, Li X-R, Preus DM, Tan L, Grunenwald H, Paulson AF, Laird DW, Sheridan JD (2002). Gap junctions assemble in the presence of cytoskeletal inhibitors, but enhanced assembly requires microtubules. Exp Cell Res 275, 67–80.
Kamasawa N *et al.* (2006). Abundance and ultrastructural diversity of neuronal gap junctions in the OFF and ON sublaminae of the inner plexiform layer of rat and mouse retina. Neuroscience 142, 1093–1117.
Laird DW (2010). The gap junction proteome and its relationship to disease. Trends Cell Biol 20, 92–101.
Lampe PD (1994). Analyzing phorbol ester effects on gap junction communication: a dramatic inhibition of assembly. J Cell Biol 127, 1895–1905.
Leithe E, Kjenseth A, Sirnes S, Stenmark H, Brech A, Rivedal E (2009). Ubiquitylation of the gap junction protein connexin-43 signals its trafficking from early endosomes to lysosomes in a process mediated by Hrs and Tsg101. J Cell Sci 122, 3883–3893.
Li X, Kamasawa N, Ciolofan C, Olson CO, Lu S, Davidson KG, Yasumura T, Shigemoto R, Rash JE, Nagy JI (2008). Connexin45-containing neuronal gap junctions in rodent retina also contain connexin36 in both apposing hemiplaques, forming bihomotypic gap junctions, with scaffolding contributed by zonula occludens-1. J Neurosci 28, 9769–9789.
Locke D, Harris AL (2009). Connexin channels and phospholipids: association and modulation. BMC Biol 7, 52.
Maass K *et al.* (2004). Defective epidermal barrier in neonatal mice lacking the C-terminal region of connexin43. Mol Biol Cell 15, 4597–4608.
Maass K, Shibayama J, Chase SE, Willecke K, Delmar M (2007). C-terminal truncation of connexin43 changes number, size, and localization of cardiac gap junction plaques. Circ Res 101, 1283–1291.
Malewicz B, Kumar VV, Johnson RG, Baumann WJ (1990). Lipids in gap junction assembly and function. Lipids 25, 419–427.
Manjunath CK, Goings GE, Page E (1987). Human cardiac gap junctions: isolation, ultrastructure, and protein composition. J Mol Cell Cardiol 19, 131–134.
Meyer RA, Laird DW, Revel J-P, Johnson RG (1992). Inhibition of gap junction and adherens junction assembly by connexin and A-CAM antibodies. J Cell Biol 119, 179–189.
Meyer RA, Lampe PD, Malewicz B, Baumann W, Johnson RG (1991). Enhanced gap junction formation with LDL and apolipoprotein B. Exp Cell Res 196, 72–81.
Paemeleire K, Martin PE, Coleman SL, Fogarty KE, Carrington WA, Leybaert L, Tuft RA, Evans WH, Sanderson MJ (2000). Intercellular calcium waves in HeLa cells expressing GFP-labeled connexin 43, 32, or 26. Mol Biol Cell 11, 1815–1827.
Paulson A, Lampe P, Meyer RA, TenBroek E, Atkinson MM, Walseth TF, Johnson RG (2000). Cyclic AMP and LDL trigger a rapid enhancement in gap junction assembly through a stimulation of connexin trafficking. J Cell Sci 113, 3037–3049.
Preus D, Johnson R, Sheridan J (1981a). Gap junctions between Novikoff hepatoma cells following dissociation and recovery in the absence of cell contact. J Ultrastruct Res 77, 248–262.
Preus D, Johnson R, Sheridan J, Meyer R (1981b). Analysis of gap junctions and formation plaques between reaggregating Novikoff hepatoma cells. J Ultrastruct Res 77, 263–276.
Rash JE *et al.* (2005). Ultrastructural localization of connexins (Cx36, Cx43, Cx45), glutamate receptors and aquaporin-4 in rodent olfactory mucosa, olfactory nerve and olfactory bulb. J Neurocytol 34, 307–341.
Rash JE, Davidson KG, Yasumura T, Furman CS (2004a). Freeze-fracture and immunogold analysis of aquaporin-4 (AQP4) square arrays, with models of AQP4 lattice assembly. Neuroscience 129, 915–934.
Rash JE, Giddings FD (1989). Counting and measuring IMPs and pits: why accurate counts are exceedingly rare. J Electron Microsc Tech 13, 204–215.
Rash JE, Pereda A, Kamasawa N, Furman CS, Yasumura T, Davidson KG, Dudek FE, Olson C, Li X, Nagy JI (2004b). High-resolution proteomic mapping in the vertebrate central nervous system: close proximity of connexin35 to NMDA glutamate receptor clusters and co-localization of connexin36 with immunoreactivity for zonula occludens protein-1 (ZO-1). J Neurocytol 33, 131–151.
Rash JE, Yasumura T (1999). Direct immunogold labeling of connexins and aquaporin-4 in freeze-fracture replicas of liver, brain, and spinal cord: factors limiting quantitative analysis. Cell Tissue Res 296, 307–321.
Rash JE, Yasumura T, Hudson CS, Agre P, Nielsen S (1998). Direct immunogold labeling of aquaporin-4 in square arrays of astrocyte and ependymocyte plasma membranes in rat brain and spinal cord. Proc Natl Acad Sci USA 95, 11981–11986.
Risinger MA, Larsen WJ (1983). Interaction of filipin with junctional membrane at different stages of the junction's life history. Tissue Cell 15, 1–15.
Shaw RM, Fay AJ, Puthenveedu MA, von Zastrow M, Jan YN, Jan LY (2007). Microtubule plus-end-tracking proteins target gap junctions directly from the cell interior to adherens junctions. Cell 128, 547–560.
Simek J, Churko J, Shao Q, Laird DW (2009). Cx43 has distinct mobility within plasma-membrane domains, indicative of progressive formation of gap-junction plaques. J Cell Sci 122, 554–562.
Sirnes S, Kjenseth A, Leithe E, Rivedal E (2009). Interplay between PKC and the MAP kinase pathway in connexin43 phosphorylation and inhibition of gap junction intercellular communication. Biochem Biophys Res Commun 382, 41–45.
Solan JL, Lampe PD (2005). Connexin phosphorylation as a regulatory event linked to gap junction channel assembly. Biochim Biophys Acta 1711, 154–163.
Solan JL, Lampe PD (2009). Connexin43 phosphorylation: structural changes and biological effects. Biochem J 419, 261–272.
Sorgen PL, Duffy HS, Sahoo P, Coombs W, Delmar M, Spray DC (2004). Structural changes in the carboxyl terminus of the gap junction protein connexin43 indicates signaling between binding domains for c-Src and zonula occludens-1. J Biol Chem 279, 54695–54701.

Sotelo C, Korn H (1978). Morphological correlates of electrical and other interactions through low-resistance pathways between neurons of the vertebrate central nervous system. Int Rev Cytol 55, 67–107.
Sotelo C, Llinas R, Baker R (1974). Structural study of inferior olivary nucleus of the cat: morphological correlates of electrotonic coupling. J Neurophysiol 37, 541–559.
Srisakuldee W, Jeyaraman MM, Nickel BE, Tanguy S, Jiang ZS, Kardami E (2009). Phosphorylation of connexin-43 at serine 262 promotes a cardiac injury-resistant state. Cardiovasc Res 83, 672–681.
Steer CJ, Bisher M, Blumenthal R, Steven AC (1984). Detection of membrane cholesterol by filipin in isolated rat liver coated vesicles is dependent upon removal of the clathrin coat. J Cell Biol 99, 315–319.
TenBroek EM, Lampe PD, Solan JL, Reynhout JK, Johnson RG (2001). Ser364 of connexin43 and the upregulation of gap junction assembly by cAMP. J Cell Biol 155, 1307–1318.
Unger VM, Kumar NM, Gilula NB, Yeager M (1999). Three-dimensional structure of a recombinant gap junction membrane channel. Science 283, 1176–1180.
Wang Y, Rose B (1995). Clustering of Cx43 cell-to-cell channels into gap junction plaques: regulation by cAMP and microfilaments. J Cell Sci 108, 3501–3508.
Warn-Cramer BJ, Lampe PD, Kurata WE, Kanemitsu MY, Loo LW, Eckhart W, Lau AF (1996). Characterization of the mitogen-activated protein kinase phosphorylation sites on the connexin-43 gap junction protein. J Biol Chem 271, 3779–3786.
Weber PA, Chang HC, Spaeth KE, Nitsche JM, Nicholson BJ (2004). The permeability of gap junction channels to probes of different size is dependent on connexin composition and permeant-pore affinities. Biophys J 87, 958–973.
Wei CJ, Xu X, Lo CW (2004). Connexins and cell signaling in development and disease. Annu Rev Cell Dev Biol 20, 811–838.